

Article

Intramolecular Hydrogen Bond, Hirshfeld Analysis, AIM; DFT Studies of Pyran-2,4-dione Derivatives

Ahmed T. A. Boraei ^{1,*}, Matti Haukka ² , Ahmed A. M. Sarhan ³, Saied M. Soliman ⁴ and Assem Barakat ^{5,*} ¹ Chemistry Department, Faculty of Science, Suez Canal University, Ismailia 41522, Egypt² Department of Chemistry, University of Jyväskylä, P.O. Box 35, FI-40014 Jyväskylä, Finland; matti.o.haukka@jyu.fi³ Chemistry Department, Faculty of Science, Arish University, Al-Arish 45511, Egypt; asarhan@aru.edu.eg⁴ Department of Chemistry, Faculty of Science, Alexandria University, P.O. Box 426, Ibrahimia, Alexandria 21321, Egypt; saeed.soliman@alexu.edu.eg⁵ Department of Chemistry, College of Science, King Saud University, P.O. Box 2455, Riyadh 11451, Saudi Arabia

* Correspondence: ahmed_boraei@science.suez.edu.eg (A.T.A.B.); ambarakat@ksu.edu.sa (A.B.); Tel.: +966-11467-5901 (A.T.A.B.); +966-11467-5992 (A.B.)

Abstract: Intra and intermolecular interactions found in the developed crystals of the synthesized pyran-2,4-dione derivatives play crucial roles in the molecular conformations and crystal stabilities, respectively. In this regard, Hirshfeld calculations were used to quantitatively analyze the different intermolecular interactions in the crystal structures of some functionalized pyran-2,4-dione derivatives. The X-ray structure of pyran-2,4-dione derivative namely (3E,3'E)-3,3'-((ethane-1,2-diylbis(azanediyl))bis(phenylmethanylylidene))bis(6-phenyl-2H-pyran-2,4(3H)-dione) was determined. It crystallized in the monoclinic crystal system and C2/c space group with unit cell parameters: $a = 14.0869(4) \text{ \AA}$, $b = 20.9041(5) \text{ \AA}$, $c = 10.1444(2) \text{ \AA}$ and $\beta = 99.687(2)^\circ$. Generally, the H...H, H...C, O...H and C...C contacts are the most important interactions in the molecular packing of the studied pyran-2,4-diones. The molecular structure of these compounds is stabilized by intramolecular O...H hydrogen bond. The nature and strength of the O...H hydrogen bonds were analyzed using atoms in molecules calculations. In all compounds, the O...H hydrogen bond belongs to closed-shell interactions where the interaction energies are higher at the optimized geometry than the X-ray one due to the shortening in the A...H distance as a consequence of the geometry optimization. These compounds have polar characters with different charged regions which explored using molecular electrostatic potential map. Their natural charges, reactivity descriptors and NMR chemical shifts were computed, discussed and compared.

Keywords: pyran-2,4-dione; Hirshfeld analysis; AIM; DFT; intramolecular hydrogen bond



Citation: Boraei, A.T.A.; Haukka, M.; Sarhan, A.A.M.; Soliman, S.M.; Barakat, A. Intramolecular Hydrogen Bond, Hirshfeld Analysis, AIM; DFT Studies of Pyran-2,4-dione Derivatives. *Crystals* **2021**, *11*, 896. <https://doi.org/10.3390/cryst11080896>

Academic Editors: Sławomir Grabowski and Ana M. Garcia-Deibe

Received: 21 June 2021

Accepted: 30 July 2021

Published: 30 July 2021

Publisher's Note: MDPI stays neutral with regard to jurisdictional claims in published maps and institutional affiliations.



Copyright: © 2021 by the authors. Licensee MDPI, Basel, Switzerland. This article is an open access article distributed under the terms and conditions of the Creative Commons Attribution (CC BY) license (<https://creativecommons.org/licenses/by/4.0/>).

1. Introduction

Heterocyclic molecules have ester oxygen functionality for example pyranones which are widely distributed in nature [1,2]. Medicinal chemistry and synthetic organic chemistry have been explored these interesting building block and versatile precursor for many divergent-targeted synthesis [3]. These active pharmacophores based on pyranones have been exploited in many pharmacologically relevant behaviors such as antitumor [4,5], anticonvulsants [6], HIV protease inhibitors [7], anti-microbial [8], antifungal [6] and plant growth regulators [7,9].

Many examples have been discovered and isolated from nature incorporating these pyranones such as Bufalin (utilized for treatment complication disordered linked with central nervous systems and others like rheumatism, and inflammations) [10]; Pectinatone (marine natural products possessed cytotoxic, antibacterial activities) [11]; Pentylpyran-2-one possessed antibiotic potency [12]; Griseulin (shown mosquitocidal and nematocidal

efficacy) [13,14]. Pyranone-based molecules have been gain of attention in the chemical research community due to pharmacological significance and their fascinating chemical structure in synthetic drug compounds as well as naturally occurring. In literature, recently the synthesis of pyranone-cored compounds have been achieved via metal-catalyzed synthetic methods [15,16], and microwave aided organic synthesis [17].

Intermolecular interactions play crucial rule in the molecular packing in the crystal structure [18]. It was believed that, little changes in the structure of compound affect the crystal structure significantly although the absence of clear relationship among them. Molecules in the crystal tend to arrange themselves in order to maximize the intermolecular interactions among them [18–21]. This molecular packing is controlled by many directional forces such as coordination interactions, hydrogen bonding, π - π stacking, C-H... π interactions and others [22–28]. Hirshfeld topology analysis is considered very important tool used to determine and quantify the intermolecular interactions in the crystal [29]. In addition, atoms in molecules (AIM) theory and the related topological parameters [30–32] are important for analyzing the nature and strength of intermolecular interactions specially the hydrogen bonding interactions.

In the light of our interest with the pyran-2,4-dione, this work aimed to shed the light on the molecular and supramolecular structural aspects of selected set of pyran-2,4-dione (Figure 1) based on X-ray single crystal structure determinations and Hirshfeld calculations, respectively. In addition, conformational analysis was performed in order to show the most sTable Structure. Atoms in molecules (AIM) study was used to explore the nature and strength of the intramolecular hydrogen bond occurred in the structure of the studied pyran-2,4-dione.

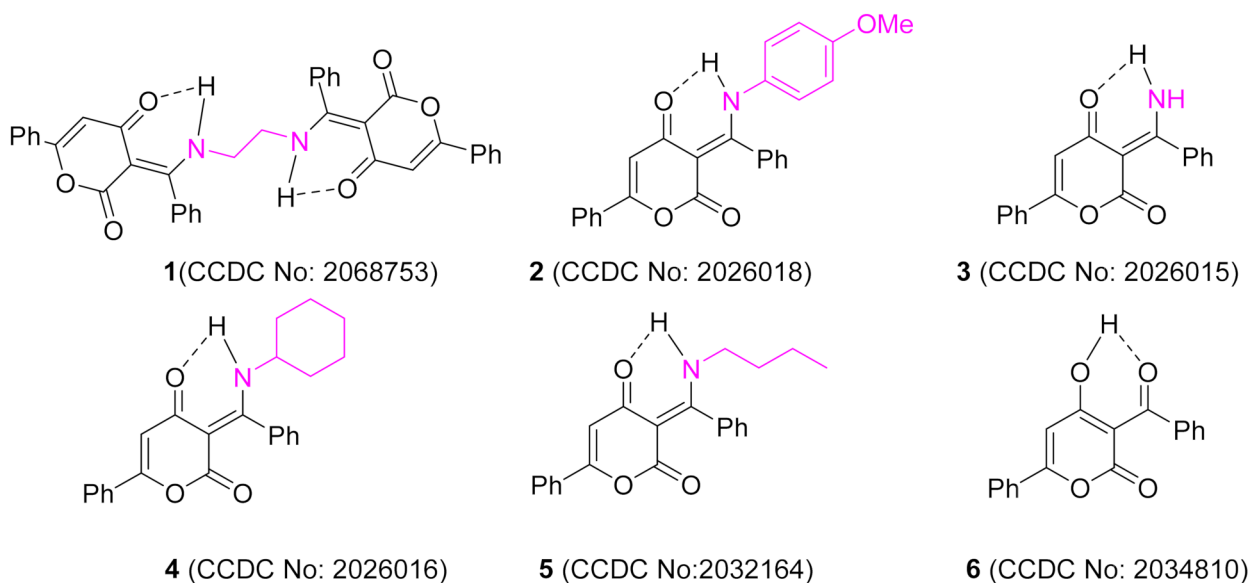


Figure 1. The structure of pyran-2,4-dione 1–6 employed in this study.

2. Materials and Methods

2.1. Synthesis

The synthesis of the studied compounds were reported in our previous published article [17]. The single crystals were grown in EtOAc: Hexane at room temperature.

2.2. X-ray Single Crystal Determination

X-ray single crystal determination details of compound 1 are provided in supplementary information.

2.3. Computational Methods

“All DFT calculations were performed using Gaussian 09 software package [33,34] utilizing B3LYP/6-31G(d,p) method. Natural bond orbital analyses were performed using NBO 3.1 program as implemented in the Gaussian 09W package [35]. The self-consistent reaction field (SCRF) method [36,37] was used to model the solvent effects when calculated the optimized geometries in solution. Then the NMR chemical shifts for the protons and carbons were computed using GIAO method in the same solvent [38]. In addition, the atoms in molecules (AIM) parameters were calculated with the aid of Multiwfn [39] program”.

3. Results and Discussion

3.1. Crystal Structure Description of (3*E*,3'*E*)-3,3'-((ethane-1,2-diylbis(azanediyl))bis(phenylmethanylylidene))bis(6-phenyl-2*H*-pyran-2,4(3*H*)-dione) **1**

The crystallographic measurement for compound **1** was performed using was collected on a Rigaku Oxford Diffraction Supernova diffractometer using Cu K α radiation (see supplementary information). The topology analyses were performed using Crystal Explorer 17.5 program [40]. The crystallographic details are summarized in Table S1 (Supplementary data).

The X-ray structure of **1** is shown in Figure 2 while the experimental bond distances and angles are listed in Table S2 (Supplementary data). The compound crystallized in monoclinic crystal system and centrosymmetric C2/c space group with lattice parameters: $a = 14.0869(4)$ Å, $b = 20.9041(5)$ Å, $c = 10.1444(2)$, $\beta = 99.687(2)^\circ$. The molecule itself possesses a center of symmetry located at the midpoint of the C19-C19 bond splitting the molecule to two equal halves. The two phenyl rings bonded to C12 showed *cis* configuration to one another where such sterically hindered conformation is stabilized by the strong intramolecular N1-H1...O1 hydrogen bonding interactions with a distance of 1.820(2) Å, resulting in a very sTable S(6) ring motif (Figure 3, upper part). The C12-N1 bond distance is found to be 1.324(2) Å, which confirm the single bond character this bond and further revealed the location of the proton H1 at the N1 atomic site rather than O1.

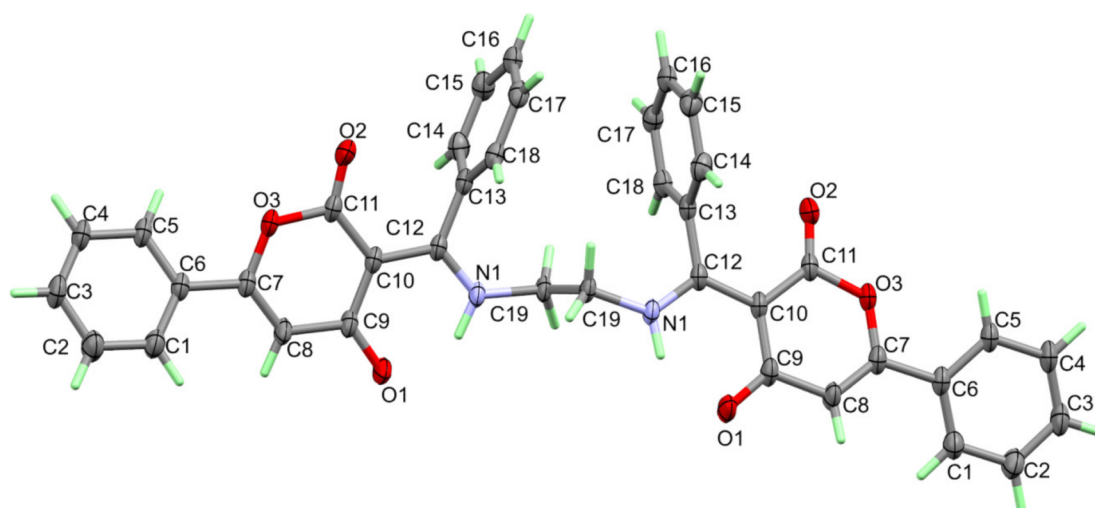


Figure 2. Structure of compound **1** with atom numbering drawn using 30% probability level for thermal ellipsoids.

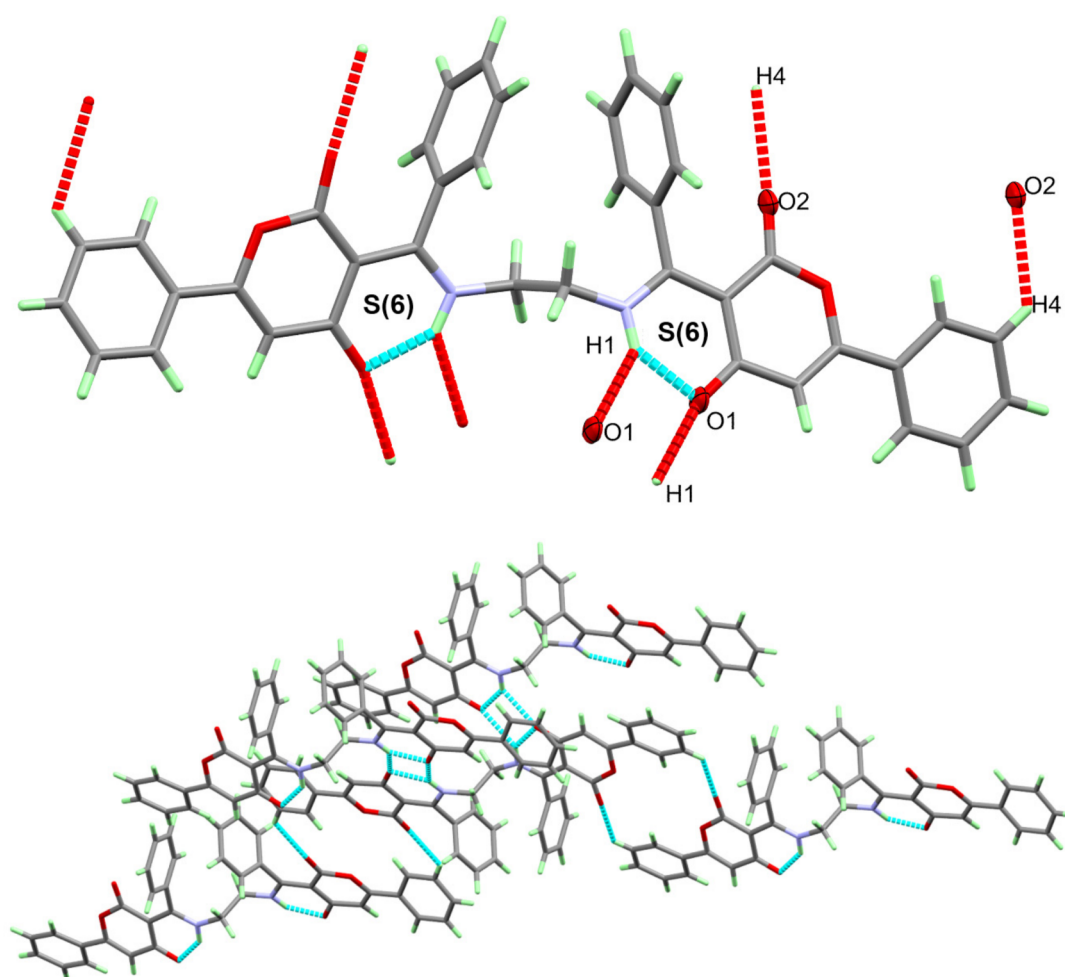


Figure 3. Hydrogen bond contacts (**upper**) and molecular packing (**lower**) via hydrogen bonding interactions for **1**.

The molecular units in the crystal lattice are packed by two intermolecular hydrogen bonding interactions shown as red dotted lines in Figure 3 (upper part). The corresponding hydrogen bond parameters are listed in Table 1. The packed molecules via the N1-H1...O1 and C4-H4...O2 hydrogen bonding interactions with donor-acceptor distances of 2.991(2) and 3.134(2) Å, respectively are shown in Figure 3 (lower part).

Table 1. Hydrogen bond parameters (Å and °) for **1**.

D-H...A	D-H	H...A	D...A	D-H...A
N1-H1...O1	0.931(19)	1.820(19)	2.593(2)	138.7(17)
N1-H1...O1 ¹	0.931(19)	2.279(19)	2.991(2)	132.8(15)
C4-H4...O2 ²	0.950	2.470	3.134(2)	127.0

Symm. Codes. ¹ 1 - x, 1 - y, 2 - z and ² 0.5 - x, 1.5 - y, 1 - z.

In addition, the molecules are packed by other contacts such as π - π stacking interactions between the pyran-dione moiety from one molecule with another pyran-dione and phenyl moieties from neighboring molecular units (Figure 4; upper part). The corresponding shortest C...C distances are C9...C9 (3.340 Å) and C2...C8 (3.351 Å), respectively. Another type of contacts which affect the molecular packing is the C-H... π interactions (Table 2). The upper part of Figure 4 shows the molecular packing in the crystal structure *via* these short C...C and C-H... π contacts.

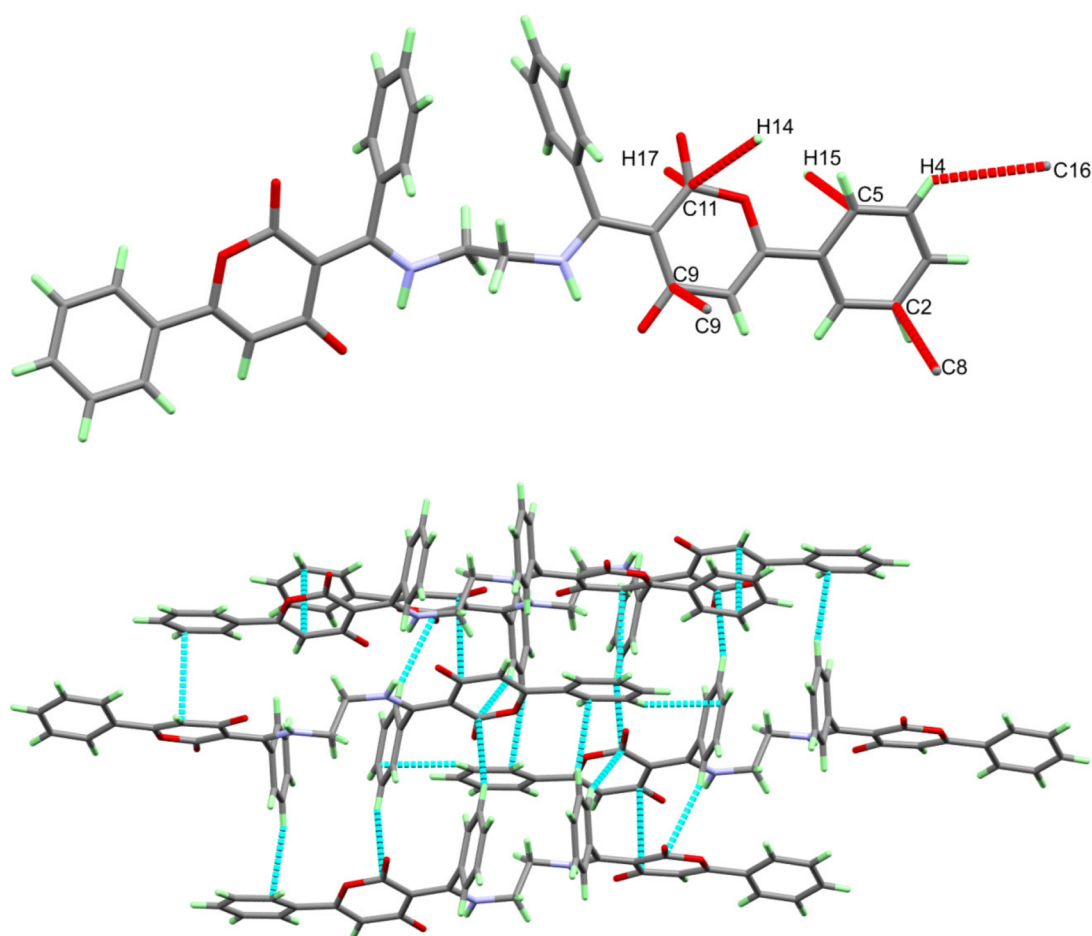


Figure 4. Other H...C and C...C contacts (**upper**) and molecular packing (**lower**) via these interact Table 1.

Table 2. Other important contacts and the corresponding interaction distances (Å) for **1**.

Contact	Length	Symm. Code.
C9...C9	3.340	$1 - x, y, 1.5 - z$
C11...H14	2.855	$1 - x, y, 2.5 - z$
C2...C8	3.351	$x, 1 - y, -1/2 + z$
C5...H15	2.724	$-1/2 + x, 1.5 - y, -1/2 + z$
C11...H17	2.762	$1/2 - x, 1.5 - y, 2 - z$
H4...C16	2.886	$1/2 - x, 1.5 - y, 1 - z$

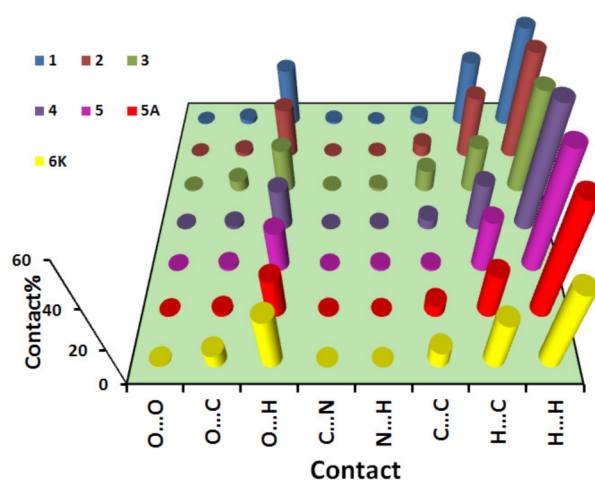
3.2. Analysis of Molecular Packing

Intermolecular interactions in the solid state structure play very important rule in the crystal stability. In this regard, we employed Hirshfeld surface analysis for decomposing the different intermolecular contacts in the crystal structure the studied systems. The results of the quantitative analysis of all possible intermolecular interactions are shown in Figure 5 while the complete Hirshfeld surfaces are given in Figures S1–S6 (Supplementary data).

Table 3. The contact percentages in the crystal structure of the studied compounds.

Contact	1 ^a	2 ^b	3 ^c	4 ^d	5	5B ^e	6K ^e
O...O	0.2	0	0.3	0.1	0	0	0.4
O...C	1.9	1.6	4.7	1.3	1.2	1.4	6.3
O...H	24.4	21.4	19.1	18.2	18.7	18.3	24.7
C...N	0.8	0	0.5	0	0.3	0.3	0
N...H	0	0.3	1.2	0.6	1	0.2	0
C...C	3.1	5.1	9.7	4.4	1	5.8	8
H...C	27.8	26.5	20.2	21	23.8	20.7	22.9
H...H	41.8	45	44.3	54.4	54	53.4	37.7

^a CCDC: 2068753; ^b CCDC: 2026018; ^c CCDC: 2026015; ^d CCDC:2026016; ^e The letters B and K refer to the atom numbering in the crystal structure with CCDC numbers 2032164 and 2034810, respectively.

**Figure 5.** Summary of the intermolecular interactions and their percentages in the crystal structure of the studied compounds. For contact percentages see Table 3.

In the newly presented structure, the molecules are arranged in the crystal via H...H (41.8%), H...C (27.8%), O...H (24.4%) and C...C (3.1%) short contacts. Presentation of the decomposed d_{norm} maps and fingerprint plots for these interactions are shown in Figure 6 while list of the most important short contacts are listed in Table 4.

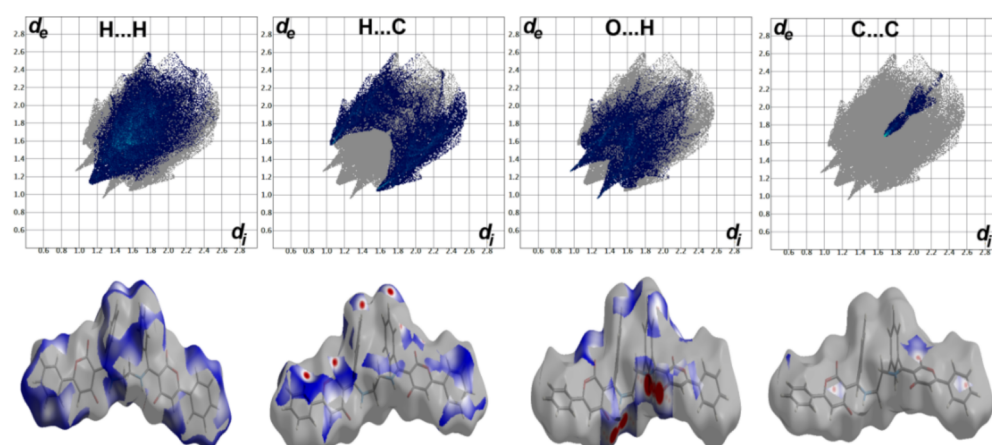
**Figure 6.** Decomposed fingerprint plots and d_{norm} Hirshfeld surfaces of the most abundant interactions in 1.

Table 4. The most important intermolecular contacts based on Hirshfeld calculations in the studied systems ^a.

1		2		3		4		5		6	
Contact	Distance	Contact	Distance	Contact	Distance	Contact	Distance	Contact	Distance	Contact	Distance
H14...C11	2.729	O2...H23C	2.190	H1...C15	2.712	H22A...C16	2.77	H17...H20C	1.986	O2J...H17K	2.598
H15...C5	2.608	O3...H2	2.145	O1...H4	2.446	H22A...C17	2.623	H17B...C7B	2.682	O2J...H18K	2.514
H17...C11	2.647	H14...C9	2.752	O2...H18	2.368	H21B...H21B	2.441	H4...C17B	2.768	O2K...H5C	2.337
O2...H4	2.390	H14...C10	2.760	O2...H2A	1.885	H16...H22A	2.44	H19D...C7	2.687	O4K...H8J	2.222
O1...H1	2.222	H20...C8	2.631	C3...C4	3.524	O2...H4	2.453	O2...H15B	2.469	O1J...H1K	2.491
O1...H19B	2.559	C5...C10	3.425	C2...C5	3.516	O2...H17	2.431	O2...H4B	2.569	O4B...H8K	2.184
C9...C9	3.340	C5...C11	3.464	C1...C6	3.524	O3...H15	2.456	O1...H20C	2.603	C6K...C8L	3.392
C2...C8	3.351	C4...C10	3.494			C2...C10	3.252	O1...H1M	2.307	H15K...H17L	2.049
		C7...C7	3.490			C2...C11	3.37	O1B...H1N	2.280		
		C19...O3	3.086					O2B...H4	2.463		
								O2B...H15	2.533		
								C11B...C2B	3.390		
								C2B...C10B	3.326		

^a Values in red for contacts with longer distances than the VDWs radii sum.

The shortest O...H contacts are O2...H4, O1...H1 and O1...H19B with contact distances of 2.390, 2.222 and 2.559 Å, respectively. Interestingly, the molecular packing is also controlled by some C-H... π interactions with interaction distances ranging from 2.647 to 2.729 Å. In addition, some π - π stacking interactions were noted with interaction distances of 3.340 Å (C9...C9) and 3.351 Å (C2...C8). These short interactions appeared as red regions in the d_{norm} map with the characteristic features for the short contacts in the fingerprint plot. In contrast, the H...H contacts contributed significantly in the crystal packing by 41.8% from the whole fingerprint area but these interactions have larger distances than the VDWs radii sum of two hydrogen atoms. Similarly, the O...O, C...O and C...N contacts have long interactions distances and small contribution in the fingerprint area.

For compound **2**, the molecular packing is controlled by short O...H (21.4%), H...C (26.5%) and C...O (1.6%) contacts in addition to the slightly long C...C (5.1%) interactions (Figure 7). The shortest contact distances are 2.145 (O3...H2), 2.631 (H20...C8), 3.086 Å (C19...O3) and 3.425 Å (C5...C10), respectively. The latter is longer than the VDWs radii sum of two carbon atoms. The H...H interactions contributed significantly in the molecular packing by 45.0% from the whole fingerprint area. Other intermolecular interactions are shown in Figure 5 such as N...H interactions are less important.

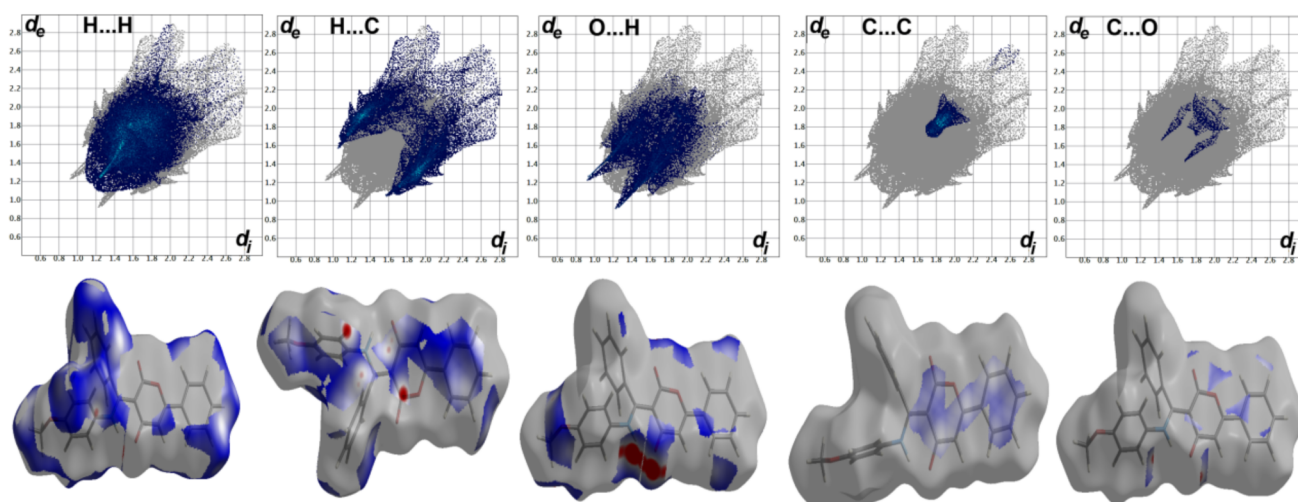


Figure 7. Decomposed fingerprint plots and d_{norm} Hirshfeld surfaces of the most abundant interactions in **2**.

Similar to **1**, the packing in compound **3** is controlled by short O...H (19.1%), H...C (20.2%) and C...C (9.7%) contacts in addition to the common H...H contacts (44.3%) which are found in all compounds presented in this publication (Figure 8). The H1...C15 (2.712 Å), O2...H2A (1.885 Å) and C2...C5 (3.516 Å) are the shortest. The H...H interactions are generally long and appeared weak so have less importance in the molecular packing of this molecule in the crystal.

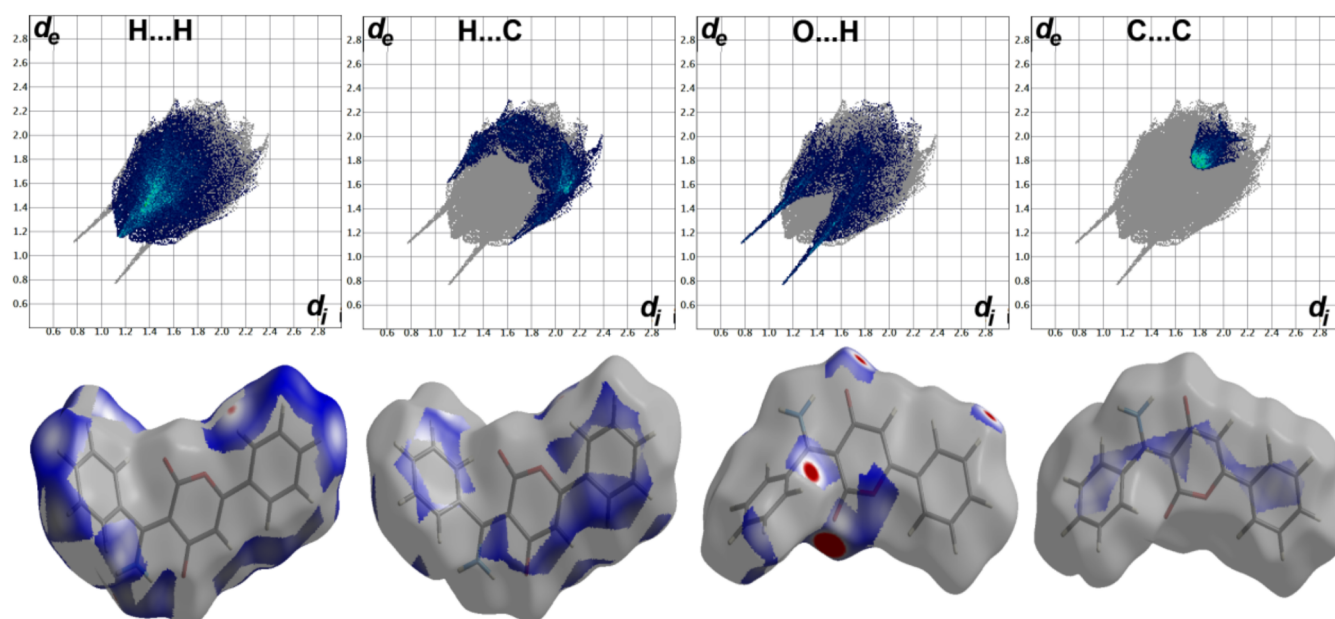


Figure 8. Decomposed fingerprint plots and d_{norm} Hirshfeld surfaces of the most abundant interactions in **3**.

In case of compound **4**, the percentages of the O...H, H...C, H...H and C...C contacts are 18.2, 21.0, 4.4 and 54.4%, respectively using Hirshfeld calculations. All appeared significant with interaction distances shorter than the VDWs radii sum of the two atoms included in these interactions except the H...H contacts which are slightly longer than the sum of the VDWs radii of two hydrogen atoms (Figure 9). The shortest interaction distances are O2...H17 (2.431 Å), H22A...C17 (2.623 Å), H16...H22A (2.44 Å) and C2...C10 (3.252 Å), respectively.

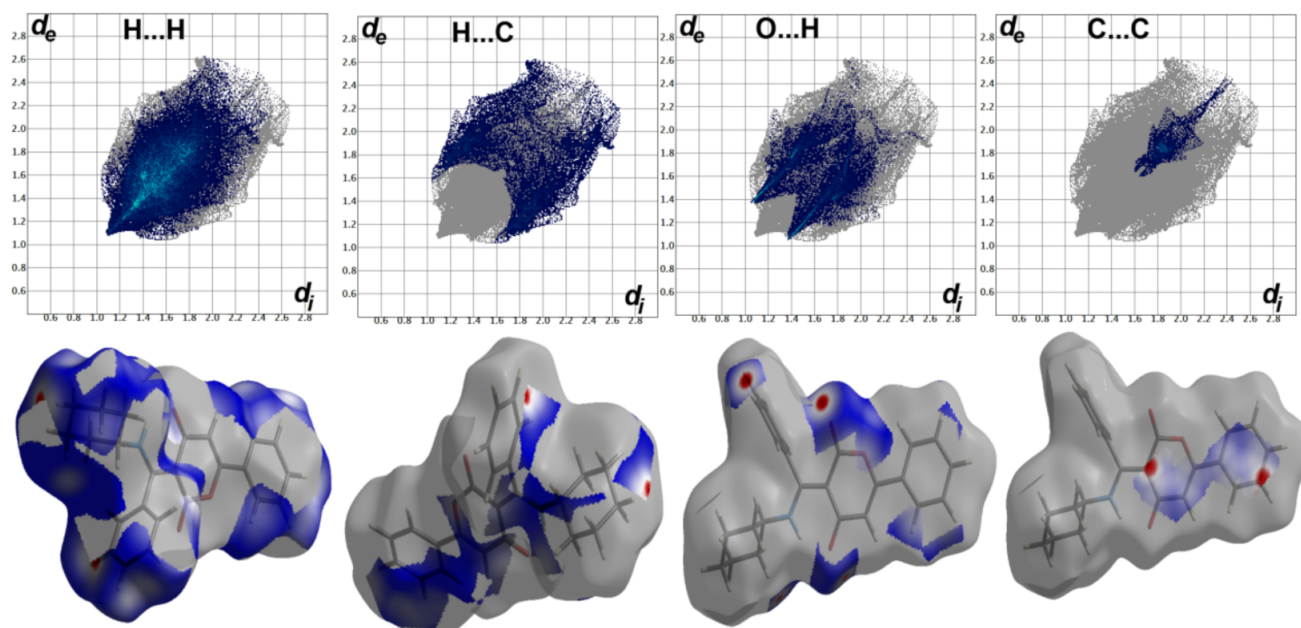


Figure 9. Decomposed fingerprint plots and d_{norm} Hirshfeld surfaces of the most abundant interactions in **4**.

In case of compound **5**, there are two different molecules per asymmetric unit hence the Hirshfeld surface and fingerprint plots shown in Figure 10 are presented for the two molecular units in the crystal. The contacts in both molecules are common in both molecular

units but showed some differences (Table 3). The H...H, H...C, O...H and C...C contacts in the crystal of 5 (without letter B in atom label) are in the range of 53.0, 23.8, 18.7 and 1.0, respectively. The corresponding values in 5B (with letter B in atom label) are 53.4, 20.7, 18.3 and 5.8%, respectively. The interactions distances of the different short contacts are listed in Table 4. The H...C interactions are in the range of 1.986 Å (H17...H20C) to 2.768 Å (H4...C17B) while for O...H contacts, the interactions ranges from 2.280 Å (O1B...H1N) to 2.603 Å (O1...H20C). Two short C...C contacts were detected which are C2B...C10B (3.326 Å) and C11B...C2B (3.390 Å) in this compound.

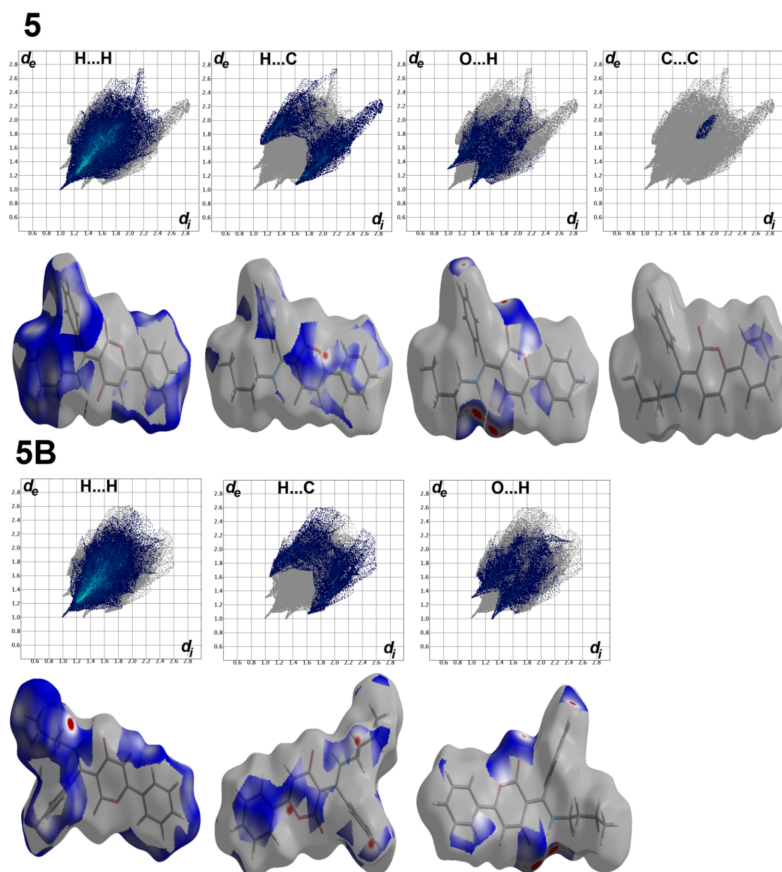


Figure 10. Decomposed fingerprint plots and d_{norm} Hirshfeld surfaces of the most abundant interactions for both units in 5. 5 and 5B refer to the atom numbering of molecular units in CIF.

The X-ray structure of 6 comprised twelve molecular units as symmetric unit as shown in the Hirshfeld d_{norm} maps presented in Figure 11. Details regarding all intermolecular interactions and their percentages for the different molecular units are listed in Table 5. The H...C, H...H and O...H as well as the C...C contacts are the major contacts in the crystal. These contacts are common for all molecular units but differently contributed in the molecular packing. For example the H...C contacts are the minimum (21.4%) in unit 6F while the maximum (23.4%) in 6D. Also, the minimum O...H contacts occurred in unit 6C (22.4%) while it is the maximum in 6I (25.2%). Decomposed fingerprint plots and d_{norm} Hirshfeld surfaces of the most abundant interactions for one molecular unit are presented in Figure 12.

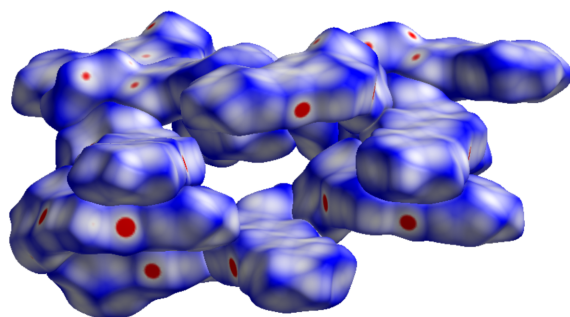


Figure 11. Hirshfeld d_{norm} surfaces of the twelve molecular units per asymmetric unit of **6**.

Table 5. All contacts and their percentages for the twelve molecular units in the crystal structure of **6**^a.

Contact	% Contact											
	6A	6B	6C	6D	6E	6F	6G	6H	6I	6J	6K	6L
O...O	0.4	0.7	0.6	0.5	0.8	0.6	0.4	0.7	0.6	0.5	0.4	0.3
O...C	6.7	5.9	6.7	6.8	4.7	5.9	6.5	5.8	4.7	5.8	6.3	6.7
O...H	24.1	23.5	22.4	24.0	25.1	23.7	24.6	23.5	25.2	24.0	24.7	22.9
C...C	8.1	9.9	9.7	8.4	8.8	9.4	8.0	9.7	9.0	9.5	8.0	9.8
H...C	23.5	23.3	21.8	23.8	22.2	21.4	23.3	23.6	21.8	22.1	22.9	22.5
H...H	37.2	36.7	38.8	36.5	38.4	39.0	37.2	36.7	38.7	38.1	37.7	37.8

^a The letters from A to L refer to the atom numbering in the crystal structure with CCDC number 2034810.

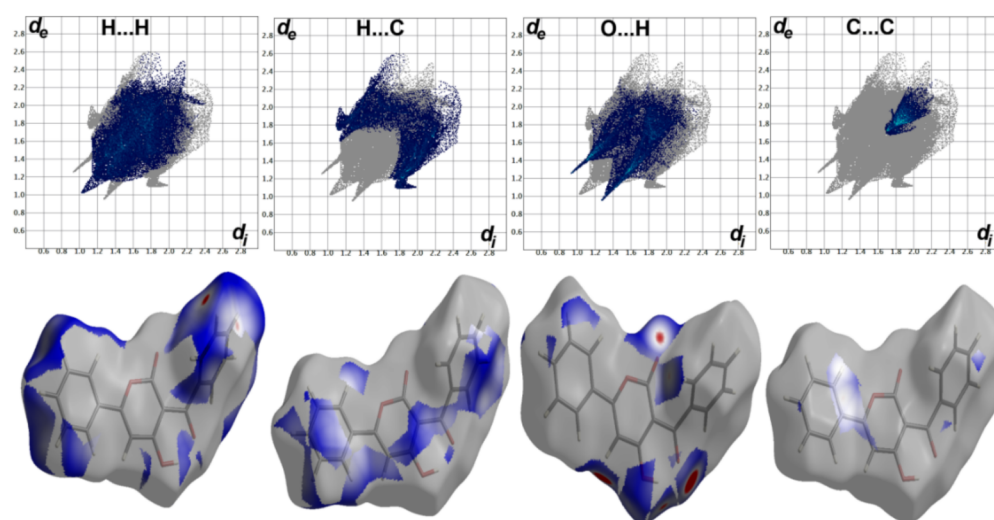


Figure 12. Decomposed fingerprint plots and d_{norm} Hirshfeld surfaces of the most abundant interactions for **6K**.

3.3. DFT Studies

The optimized geometries of the studied molecules are shown in Figure 13 along with their overlay with the experimental ones. Generally, there is good structure matching between the optimized and experimental ones. Some variations between the calculated and experimental structures could be attributed to the crystal packing effects (Tables S3–S8, Supplementary data). Generally, good correlations between the calculated and experimental bond distances and angles (Figure 14) were obtained.

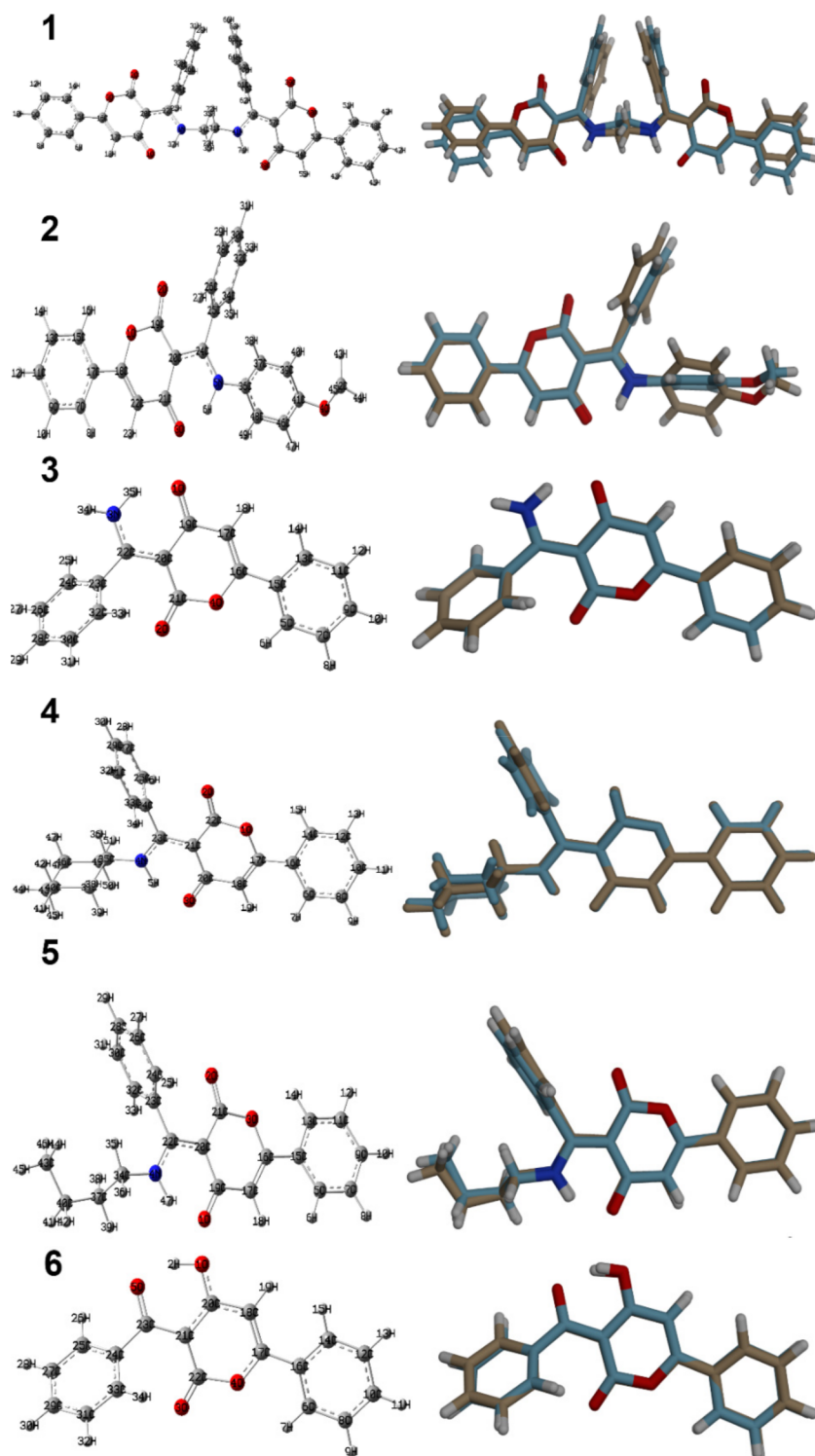


Figure 13. The optimized geometry (left) and overlay of the optimized with experimental structures, (right) for the studied molecules.

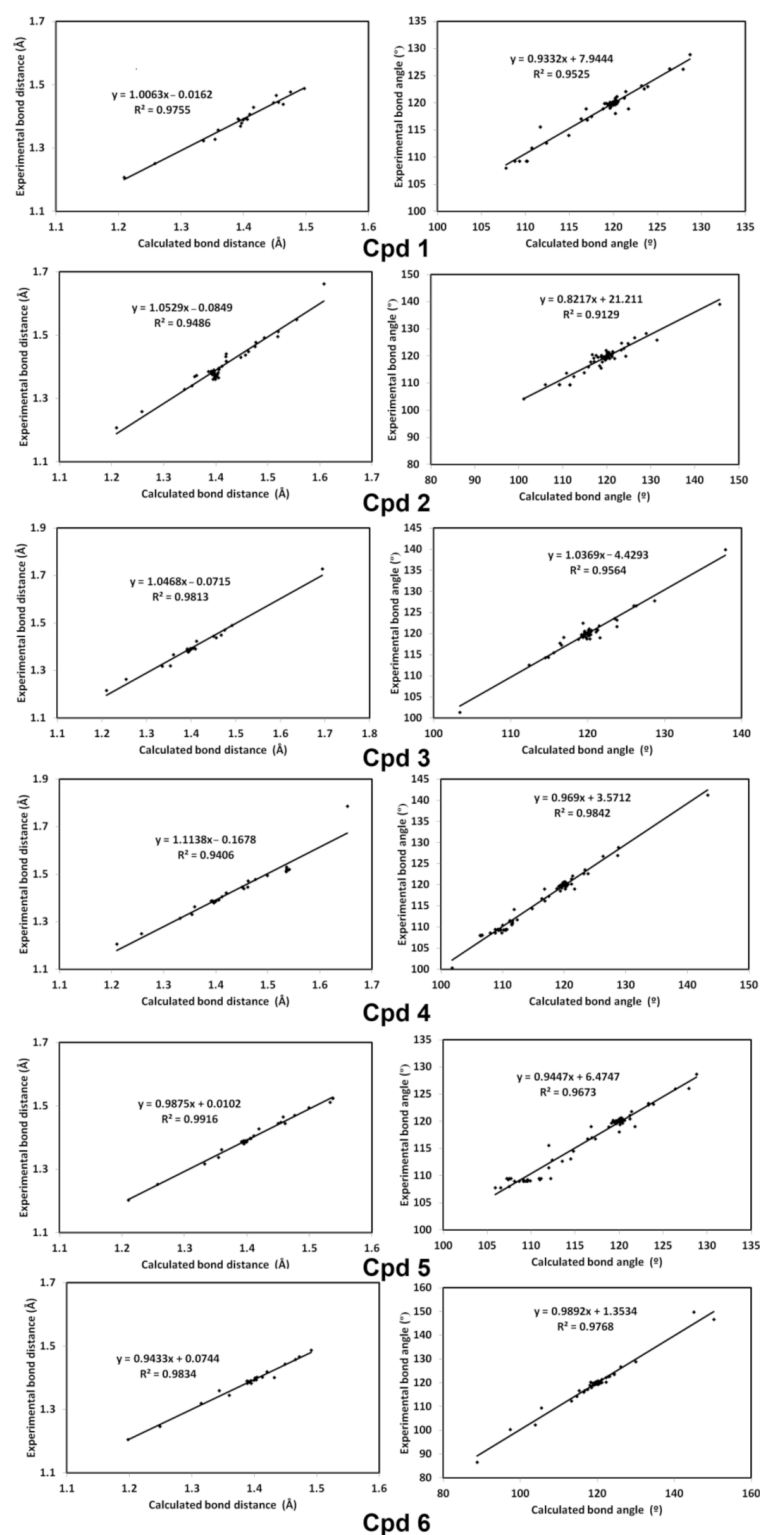


Figure 14. The straight line correlations between the calculated and experimental geometric parameters. Detailed geometric parameters (bond distances and angles are listed in Tables S3–S8, Supplementary data).

Natural charge calculations at the different atomic sites are calculated using NBO method and the results are given in Table S9 (Supplementary data). The pyran-2,4-dione derivatives have electronegative heterocyclic oxygen atom with natural charge ranging from $-0.524 e$ for compound 2 to $-0.530 e$ for compound 6. The two carbonyl oxygen atoms

have also negative charge ranging from -0.563 (compound 1) to -0.582 (compound 4) for the carbonyl group at 2-position while ranging from -0.641 e (Compound 4) to -0.649 (compound 4) for the carbonyl group at 4-position. The majority of carbon atoms are also electronegative except those attached to O or N sites. In contrast, all hydrogen atoms are positively charged with maximum natural charges at the OH and NH protons. The natural charges at these hydrogen sites is the maximum for the NH proton in compound 3 (0.462 e) while the least for the OH proton in compound 1 (0.494 e). Due to the presence of differently charged regions, the studied molecules have polar nature with dipole moment ranging from 0.1786 Debye for compound 1 to 3.4590 Debye for compound 6. Presentation of the total electron density mapped with molecular electrostatic potential for the studied molecules showing the positively charge regions in blue colored area while the most negative regions have red color is shown in Figure 15.

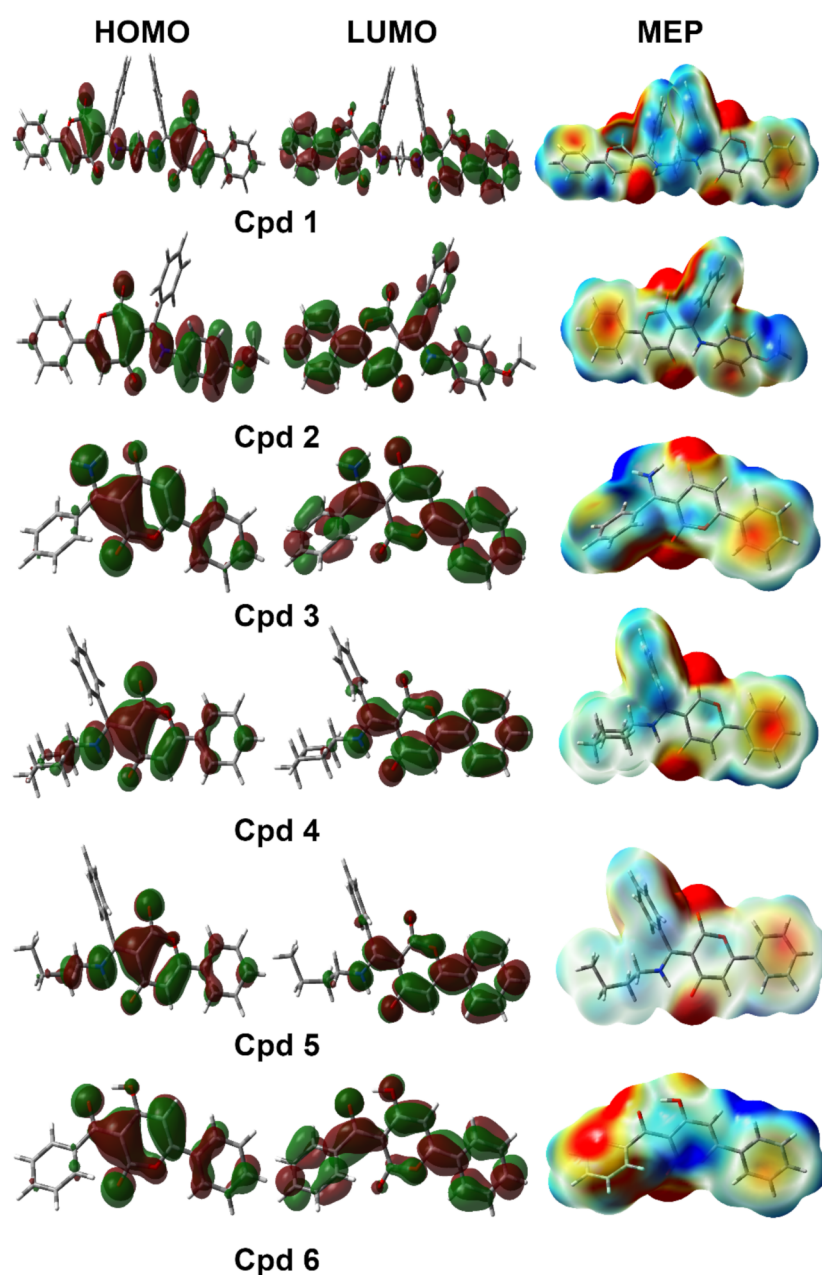


Figure 15. The MEP, HOMO and LUMO of the studied molecules. In MEP the red and blue colors indicate the most negative and most positive regions, respectively.

In the same figure, the HOMO and LUMO levels for the studied pyran-2,4-dione are presented. Both molecular orbitals (MOs) are distributed over the π -system of the studied molecules indicating HOMO→LUMO excitation based mainly on π - π^* excitation (Figure 15). In addition, the energies of these MOs are used to calculate the different reactivity descriptors [41–47] such as ionization potential (I), electron affinity (A), hardness (η), electrophilicity index (ω) and chemical potential (μ). The results listed in Table 6 indicated that **6** has the highest ionization potential, electron affinity, electronegativity and electrophilicity index while the lowest chemical potential. In addition, compound **5** is the hardest among the studied series.

Table 6. Reactivity descriptors for the studied systems.

Parameter	1	2	3	4	5	6
I	6.0241	5.5846	6.0755	5.8559	5.8932	6.6029
A	2.0052	1.9516	1.9606	1.7307	1.7647	2.6314
η	4.0189	3.6330	4.1149	4.1253	4.1285	3.9715
μ	−4.0147	−3.7681	−4.0181	−3.7933	−3.8289	−4.6171
x	4.0147	3.7681	4.0181	3.7933	3.8289	4.6171
ω	2.0052	1.9541	1.9617	1.7440	1.7755	2.6838

3.4. NMR Spectra

The NMR chemical shifts for the protons and carbons were computed using GIAO method and applying the solvent model. The results of the proton and carbon chemical shifts were collected in Tables S10–S15 (Supplementary data). Correlations between the experimental [17] and calculated results are shown in Figure 16. As clearly seen from these correlation graphs, there are good correlations between the calculated and experimental data where the correlation coefficients are very close to 1.

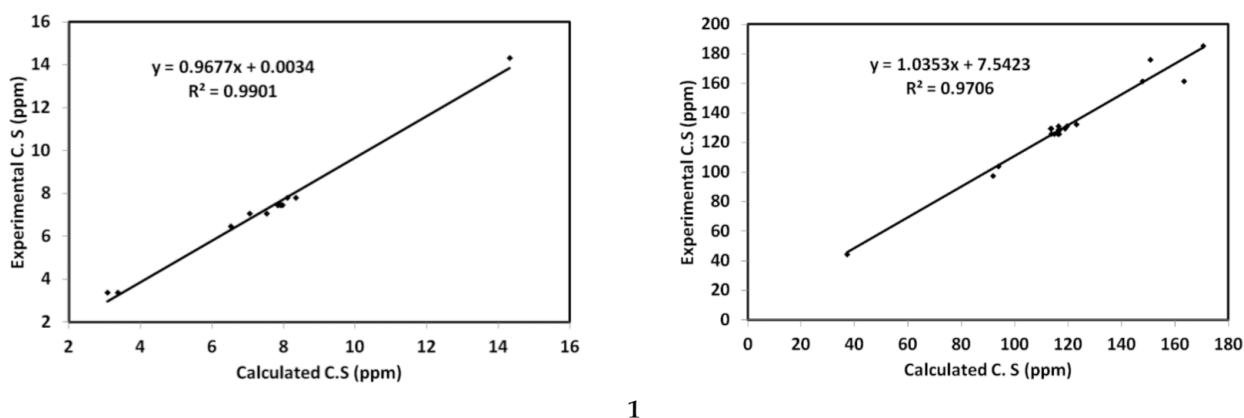
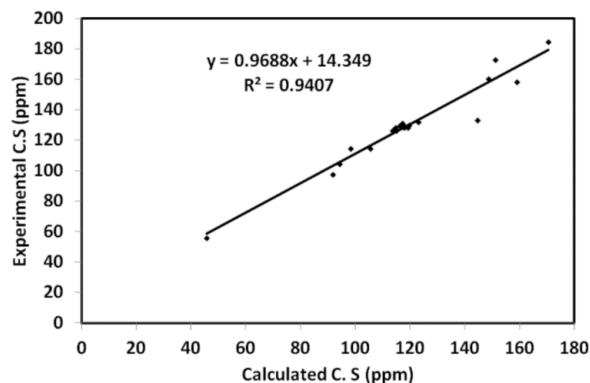
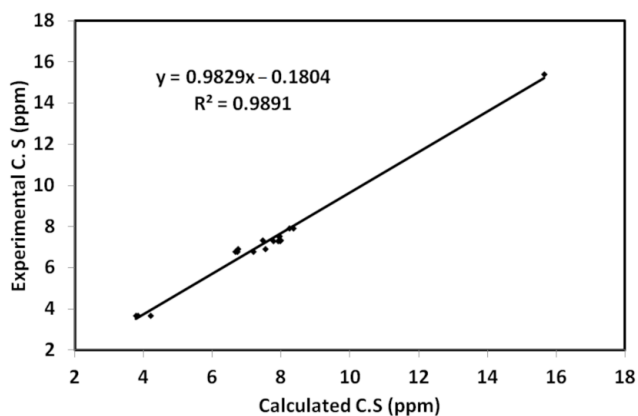
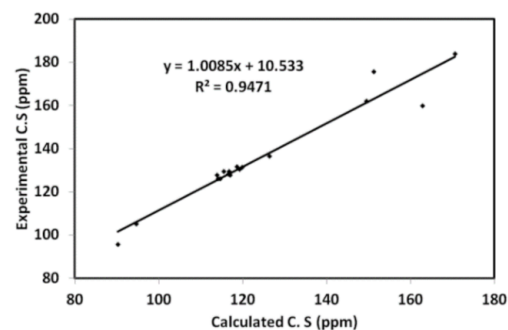
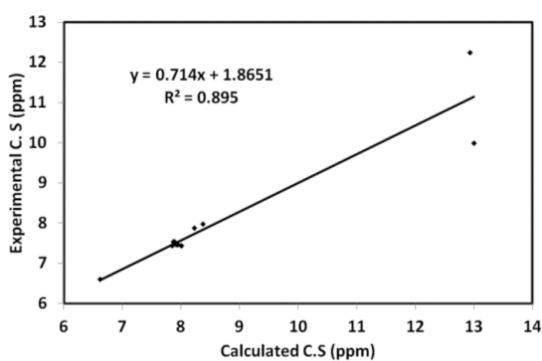


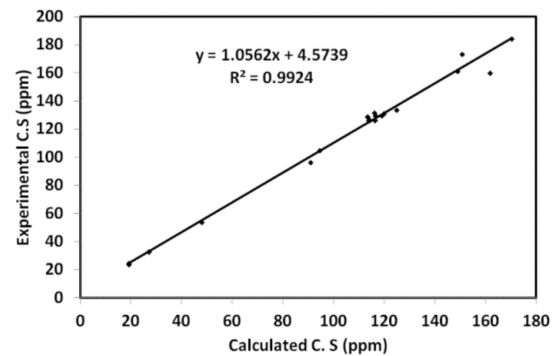
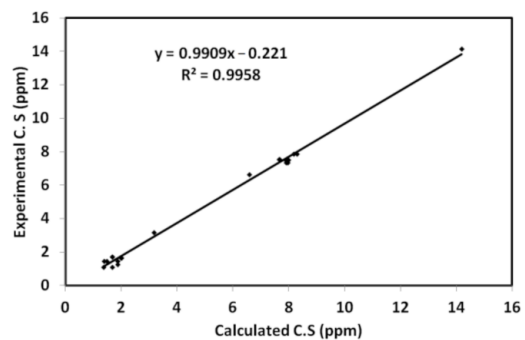
Figure 16. Cont.



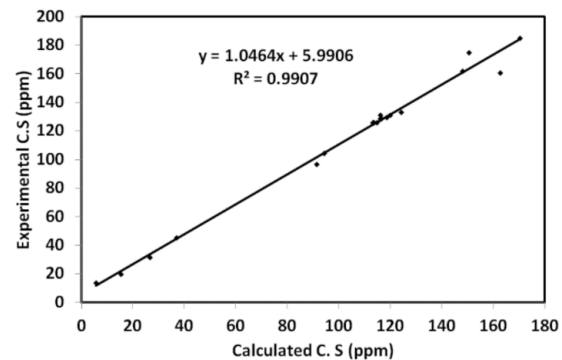
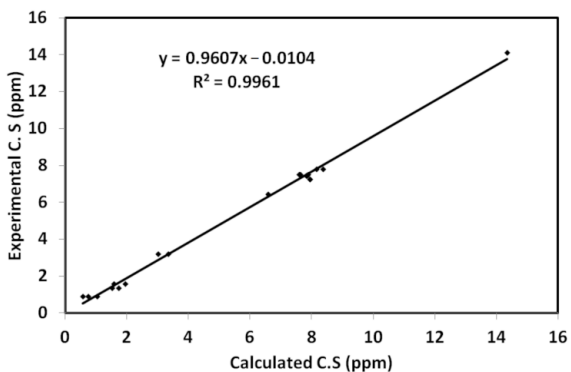
2



3

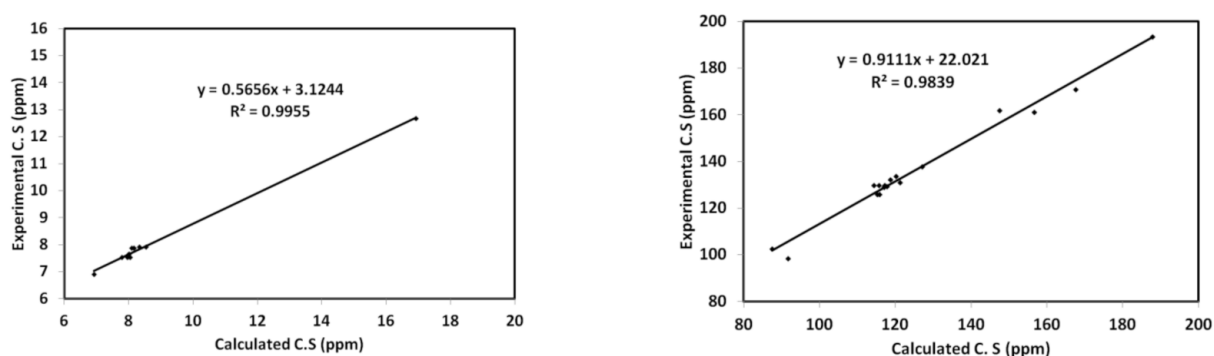


4



5

Figure 16. Cont.



6

Figure 16. Correlations between the experimental and calculated chemical shifts for the studied compounds. 1–6 are described in Figure 1.

3.5. Conformational Analysis

The presence of more than one possible conformer or tautomer is common in literature in many organic systems [48,49]. The X-ray of the pyran-2,4-dione derivatives revealed that their molecular structures stabilized by intramolecular O-H...O or N-H...O hydrogen bonding interactions. In these structures there are two possible isomers for each compound as shown in Figure 17. Energy and thermodynamic calculations of the two suggested isomers of the studied pyran-2,4-diones were used in order to compare their relative stabilities. The calculations revealed that form **A** is the most stable form and has the lowest energy compared to **B** (Table S16). Also, the more negative value of the Gibbs free energy of isomer **A** compared to **B** indicated that the former is the most stable thermodynamically. Interestingly, the optimization of **15(B)** ended to the same optimized geometry of **15(A)** which further confirm the extrastability of the pyran-2,4-dione (**A**) form over the pyran-2-one isomer (**B**) which agree with the reported X-ray structure of these compounds [17].

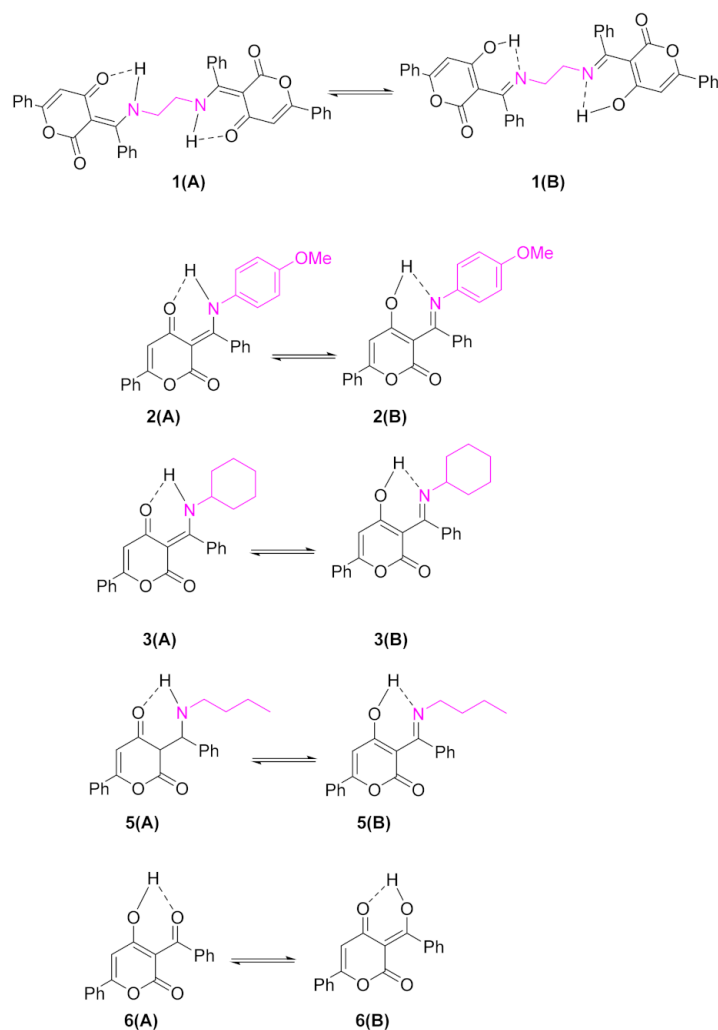


Figure 17. The suggested isomers of the studied pyran-2,4-dione.

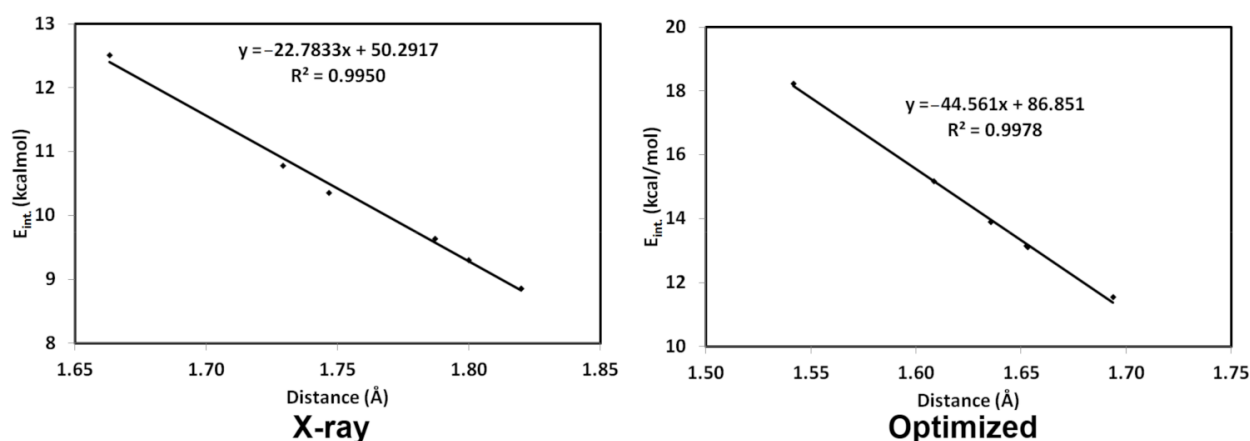
3.6. AIM Study

Atoms in molecules theory (AIM) [19,50] is a popular approach used for describing various inter- and intramolecular interactions efficiently. The AIM topological parameters such as electron density ($\rho(r)$), kinetic energy density $G(r)$, potential energy density $V(r)$ and total electron energy density ($H(r) = V(r) + G(r)$), at the bond critical point (BCP) of interaction atoms or fragments [51–53] are important for describing the nature and strength of interaction. Generally, the shared interactions have $\rho(r)$ should be $>10^{-1}$ a.u. while closed-shell interactions have $\rho(r) \approx 10^{-2}$. Hence, $\rho(r)$ is a measure for the degree of covalency in the intermolecular interactions [21]. In addition, Espinosa [54] interaction energy ($E_{\text{int}} = 1/2 (V_{\text{BCP}})$) is a measure of the strength of intermolecular interactions.

The molecular structures of all systems under investigation are stabilized by intramolecular O...H hydrogen bond. All intramolecular O...H hydrogen bonds have $\rho(r)$ less than 0.1 a.u. which is typical for closed-shell interactions [55–57]. As shown in Table 7, the values of electron density ($\rho(r)$) of bond critical points are in the range 0.0345–0.0492 a.u. and 0.0228–0.0639 at the X-ray and optimized structure, respectively. The H-bonding interaction energies (E_{int}) are generally higher at the optimized geometry than the X-ray one which is attributed to the further relaxation of the donor-hydrogen distance which of course lead to shortening the acceptor (A)...hydrogen (H) distances. The correlation between A...H distances and E_{int} gave straight lines with high correlation coefficient ($R^2 = 0.95\text{--}0.998$) with negative slope indicating higher E_{int} for shorter A...H distance (Figure 18).

Table 7. The AIM results for the intramolecular O...H hydrogen bond in the studied compounds.

Compound	ρ	G(r)	K(r)	V(r)	E _{int}	H(r)	V(r)/G(r)
1 ^a	0.0345	0.0301	−0.0019	−0.0282	8.8605	0.0019	0.9381
	0.0345	0.0301	−0.0019	−0.0282	8.8605	0.0019	0.9381
1 ^b	0.0527	0.0427	0.0016	−0.0443	13.8994	−0.0016	1.0374
	0.0527	0.0427	0.0016	−0.0443	13.8994	−0.0016	1.0374
2 ^a	0.0492	0.0391	0.0008	−0.0399	12.5176	−0.0008	1.0215
2 ^b	0.0564	0.0454	0.0030	−0.0484	15.1860	−0.0030	1.0661
3 ^a	0.0420	0.0356	−0.0013	−0.0344	10.7834	0.0013	0.9642
3 ^b	0.0228	0.0371	−0.0003	−0.0368	11.5526	0.0003	0.9925
4 ^a	0.0371	0.0327	−0.0020	−0.0307	9.6382	0.0020	0.9381
4 ^b	0.0505	0.0409	0.0010	−0.0419	13.1582	−0.0010	1.0250
5 ^a	0.0361	0.0315	−0.0019	−0.0297	9.3043	0.0019	0.9408
5 ^b	0.0504	0.0408	0.0010	−0.0418	13.1161	−0.0010	1.0236
6 ^a	0.0391	0.0353	−0.0023	−0.0330	10.3558	0.0023	0.9352
6 ^b	0.0639	0.0499	0.0082	−0.0581	18.2446	−0.0082	1.1650

^a X-ray, ^b Opt.**Figure 18.** Inverse correlations between E_{int} and A...H distance.

In addition, the total energy density (H(r)) [58] and $|V(r)|/G(r)$ ratio [59] are positive and less than 1 for closed-shell interactions while the opposite is true for covalent interactions. The results shown in Table 7 shed the light on the little covalent character for the studied intramolecular hydrogen bonding interactions.

4. Conclusions

X-ray crystal structure of pyran-2,4-dione derivative **1** was unambiguously confirmed. Its supramolecular structure was compared with a series of pyran-2,4-dione derivatives using Hirshfeld calculations. Different intermolecular interactions such as H...H, H...C, O...H and C...C contacts are of high importance in the molecular packing of the studied pyran-2,4-dione derivatives. DFT calculation revealed that the 2,4-dione isomers are the most stable in accord with the X-ray structure. The molecular structure of these compounds are stabilized by intramolecular O...H hydrogen bond which belong to closed-shell interactions according to AIM calculations where the hydrogen bonding interaction energies are generally higher at the optimized geometry than the X-ray one. Excellent correlations were obtained between A...H distances and E_{int}. At the molecular level, all compound are polar molecules with dipole moment ranging from 0.1786 to 3.4590 Debye for compounds **1** and **6**, respectively. In addition, the calculated NMR chemical shifts showed good correlation with the experimental data.

Supplementary Materials: The following are available online at <https://www.mdpi.com/article/10.3390/cryst11080896/s1>, X-ray single crystal determination of **1**; Figure S1 Hirshfeld surfaces of **1**; Figure S2 Hirshfeld surfaces of **2**; Figure S3 Hirshfeld surfaces of **3**; Figure S4 Hirshfeld surfaces of **4**; Figure S5 Hirshfeld surfaces of **5**; Figure S6 Hirshfeld surfaces for one molecular unit of **6**; Table S1 Crystal data and structure refinement for **1**; Table S2 Bond lengths (Å) and angles (°) for **1**; Table S3 The calculated geometric parameters of **1**; Table S4 The calculated geometric parameters of **2**; Table S5 The calculated geometric parameters of **3**; Table S6 The calculated geometric parameters of **4**; Table S7 The calculated geometric parameters of **5**; Table S8 The calculated geometric parameters of **6**; Table S9 Natural charges (NC) at the different atomic sites in the studied molecules; Table S10 The calculated and experimental NMR chemical shifts of **1**; Table S11 The calculated and experimental NMR chemical shifts of **2**; Table S12 The calculated and experimental NMR chemical shifts of **3**; Table S13 The calculated and experimental NMR chemical shifts of **4**; Table S14 The calculated and experimental NMR chemical shifts of **5**; Table S15 The calculated and experimental NMR chemical shifts of **6**; Table S16 Calculated energies and thermodynamic parameters for the suggested isomers of the studied pyran-2,4-dione ^a.

Author Contributions: Conceptualization, A.T.A.B., S.M.S. and A.B.; synthesis and characterization, A.T.A.B. and A.A.M.S.; X-ray crystal structure carried out by: M.H.; writing original manuscript, A.T.A.B., S.M.S. and A.B.; revision and editing, A.T.A.B., S.M.S. and A.B. All authors have read and agreed to the published version of the manuscript.

Funding: Researchers Supporting Project (RSP-2021/64), King Saud University, Riyadh, Saudi Arabia.

Acknowledgments: The authors would like to extend their sincere appreciation to the Researchers Supporting Project (RSP-2021/64), King Saud University, Riyadh, Saudi Arabia.

Conflicts of Interest: The authors declare no conflict of interest.

References

1. Rateb, M.E.; Ebel, R. Secondary metabolites of fungi from marine habitats. *Nat. Prod. Rep.* **2011**, *28*, 290–344. [[CrossRef](#)] [[PubMed](#)]
2. Lee, I.-K.; Yun, B.-S. Styrylpyrone-class compounds from medicinal fungi *Phellinus* and *inonotus* spp., and their medicinal importance. *J. Antibiot.* **2011**, *64*, 349–359. [[CrossRef](#)]
3. Lee, J.S. Recent Advances in the Synthesis of 2-Pyrone. *Mar. Drugs* **2015**, *13*, 1581–1620. [[CrossRef](#)] [[PubMed](#)]
4. Boger, D.L.; Mullican, M.D. Regiospecific total synthesis of juncusol. *J. Org. Chem.* **1984**, *49*, 4045–4050. [[CrossRef](#)]
5. Rabideau, P.W.; Harvey, R.G. Metal-ammonia reduction. VII. Stereospecific reduction in the phenanthrene series. *J. Org. Chem.* **1970**, *35*, 25–30. [[CrossRef](#)]
6. Kelly, T.R.; Li, Q.; Bhushan, V. Intramolecular biaryl coupling: Asymmetric synthesis of the chiral B-ring diol unit of pramidine. *Tetrahedron Lett.* **1990**, *31*, 161–164. [[CrossRef](#)]
7. Fisch, M.; Flick, B.H.; Arditti, J. Structure and antifungal activity of hircinol, loroglossol and orchinol. *Phytochemistry* **1973**, *12*, 437–441. [[CrossRef](#)]
8. Goel, A.; Ram, V.J. Natural and synthetic 2H-pyran-2-ones and their versatility in organic synthesis. *Tetrahedron* **2009**, *65*, 7865–7913. [[CrossRef](#)]
9. Tsuchiya, K.; Kobayashi, S.; Nishikiori, T.; Nakagawa, T.; Tatsuta, K. NK10958P, a novel plant growth regulator produced by *Streptomyces* sp. *J. Antibiot.* **1997**, *50*, 259–260. [[CrossRef](#)]
10. Costa, S.S.; Jossang, A.; Bodo, B. 4'''-Acetylsagittatin A, a kaempferol triglycoside from *Kalanchoe streptantha*. *J. Nat. Prod.* **1996**, *59*, 327–329. [[CrossRef](#)]
11. Birkbeck, A.A.; Enders, D. The total synthesis of (+)-pectinatone: An iterative alkylation approach based on the SAMP-hydrazone method. *Tetrahedron Lett.* **1998**, *39*, 7823–7826. [[CrossRef](#)]
12. Parker, S.R.; Cutler, H.G.; Jacyno, J.M.; Hill, R.A. Biological Activity of 6-Pentyl-2H-pyran-2-one and Its Analogs. *J. Agric. Food Chem.* **1997**, *45*, 2774–2776. [[CrossRef](#)]
13. Nair, M.G.; Chandra, A.; Thorogood, D.L. Griseulin, a new nitro-containing bioactive metabolite produced by *Streptomyces* spp. *J. Antibiot.* **1993**, *46*, 1762–1763. [[CrossRef](#)]
14. Ishibashi, Y.; Nishiyama, S.; Yamamura, S. Structural revision of griseulin, a bioactive pyrone possessing a nitrophenyl unit. *Chem. Lett.* **1994**, *23*, 1747–1748. [[CrossRef](#)]
15. Xue, F.; Li, X.; Wan, B. A Class of Benzene Backbone-Based Olefin–Sulfoxide Ligands for Rh-Catalyzed Enantioselective Addition of Arylboronic Acids to Enones. *J. Org. Chem.* **2011**, *76*, 7256–7262. [[CrossRef](#)]
16. Gianni, J.; Pirovano, V.; Abbiati, G. Silver triflate/p-TSA co-catalysed synthesis of 3-substituted isocoumarins from 2-alkynylbenzoates. *Org. Biomol. Chem.* **2018**, *16*, 3213–3219. [[CrossRef](#)]

17. Sarhan, A.A.; Haukka, M.; Barakat, A.; Boraie, A.T. A novel synthetic approach to pyran-2,4-dione scaffold production: Microwave-assisted dimerization, cyclization, and expeditious regioselective conversion into β -enamino-pyran-2, 4-diones. *Tetrahedron Lett.* **2020**, *61*, 152660. [CrossRef]
18. Desiraju, G.R.; Steiner, T. *The Weak Hydrogen Bond in Structural Chemistry and Biology*; Oxford University Press: Oxford, UK, 1999. [CrossRef]
19. Bader, R.F.W. *Atoms in Molecules: A Quantum Theory*; Oxford University Press: Oxford, UK, 1990.
20. Bader, R.F.W. A Bond Path: A Universal Indicator of Bonded Interactions. *J. Phys. Chem. A* **1998**, *102*, 7314–7323. [CrossRef]
21. Parthasarathi, R.; Subramanian, V.; Sathyamurthy, N. Hydrogen Bonding without Borders: An Atoms-in-Molecules Perspective. *J. Phys. Chem. A* **2006**, *110*, 3349–3351. [CrossRef]
22. Rosi, N.L.; Eckert, J.; Eddaoudi, M.; Vodak, D.T.; Kim, J.; O’Keeffe, M.; Yaghi, O.M. Hydrogen storage in microporous metal-organic frameworks. *Science* **2003**, *300*, 1127–1129. [CrossRef] [PubMed]
23. Lazare, J.; Daggag, D.; Dinadayalane, T. DFT study on binding of single and double methane with aromatic hydrocarbons and graphene: Stabilizing CH...HC interactions between two methane molecules. *Struct. Chem.* **2021**, *32*, 591–605. [CrossRef]
24. Daggag, D.; Dorlus, T.; Dinadayalane, T. Binding of histidine and proline with graphene: DFT study. *Chem. Phys. Lett.* **2019**, *730*, 147–152. [CrossRef]
25. Deng, J.-H.; Luo, J.; Mao, Y.-L.; Lai, S.; Gong, Y.-N.; Zhong, D.-C.; Lu, T.-B. π - π stacking interactions: Non-negligible forces for stabilizing porous supramolecular frameworks. *Sci. Adv.* **2020**, *6*, eaax9976. [CrossRef]
26. Vušurović, J.; Breuker, K. Relative Strength of Noncovalent Interactions and Covalent Backbone Bonds in Gaseous RNA–Peptide Complexes. *Anal. Chem.* **2018**, *91*, 1659–1664. [CrossRef]
27. Daggag, D.; Lazare, J.; Dinadayalane, T. Conformation dependence of tyrosine binding on the surface of graphene: Bent pre-fers over parallel orientation. *App. Surf. Sci.* **2019**, *483*, 178–186. [CrossRef]
28. Varadwaj, P.R.; Varadwaj, A.; Marques, H.M.; Yamashita, K. Significance of hydrogen bonding and other noncovalent interactions in determining octahedral tilting in the CH₃NH₃PbI₃ hybrid organic-inorganic halide perovskite solar cell semi-conductor. *Sci. Rep.* **2019**, *9*, 50. [CrossRef]
29. Moulton, B.; Zaworotko, M.J. From molecules to crystal Engineering: Supramolecular isomerism and polymorphism in network solids. *Chem. Rev.* **2001**, *101*, 1629–1658. [CrossRef]
30. Yang, H.-B.; Das, N.; Huang, F.; Hawkrigge, A.M.; Muddiman, D.C.; Stang, P.J. Molecular Architecture via Coordination: Self-Assembly of Nanoscale Hexagonal Metallodendrimers with Designed Building Blocks. *J. Am. Chem. Soc.* **2006**, *128*, 10014–10015. [CrossRef] [PubMed]
31. Desiraju, G.R. The C–H...O hydrogen Bond: Structural implications and supramolecular design. *Acc. Chem. Res.* **1996**, *29*, 441–449. [CrossRef] [PubMed]
32. McKinnon, J.J.; Jayatilaka, D.; Spackman, M.A. Towards quantitative analysis of intermolecular interactions with Hirshfeld surfaces. *Chem. Commun.* **2007**, *37*, 3814–3816. [CrossRef] [PubMed]
33. Frisch, M.J.; Trucks, G.W.; Schlegel, H.B.; Scuseria, G.E.; Robb, M.A.; Cheeseman, J.R.; Scalmani, G.; Barone, V.; Mennucci, B.; Petersson, G.A.; et al. *GAUSSIAN 09*; Revision A02; Gaussian Inc.: Wallingford, CT, USA, 2009.
34. Dennington, R., II; Keith, T.; Millam, J. (Eds.) *GaussView*; Version 4.1.; Semichem Inc.: Shawnee Mission, KS, USA, 2007.
35. Reed, A.E.; Curtiss, L.A.; Weinhold, F. Intermolecular interactions from a natural bond orbital, donor-acceptor viewpoint. *Chem. Rev.* **1988**, *88*, 899–926. [CrossRef]
36. Marten, B.; Kim, K.; Cortis, C.; Friesner, R.A.; Murphy, R.B.; Ringnalda, M.N.; Sitkoff, D.; Honig, B. New Model for Calculation of Solvation Free Energies: Correction of Self-Consistent Reaction Field Continuum Dielectric Theory for Short-Range Hydrogen-Bonding Effects. *J. Phys. Chem.* **1996**, *100*, 11775–11788. [CrossRef]
37. Tannor, D.J.; Marten, B.; Murphy, R.; Friesner, R.A.; Sitkoff, D.; Nicholls, A.; Honig, B.; Ringnalda, M.; Iii, W.A.G. Accurate First Principles Calculation of Molecular Charge Distributions and Solvation Energies from Ab Initio Quantum Mechanics and Continuum Dielectric Theory. *J. Am. Chem. Soc.* **1994**, *116*, 11875–11882. [CrossRef]
38. Cheeseman, J.R.; Trucks, G.W.; Keith, T.A.; Frisch, M.J. A comparison of models for calculating nuclear magnetic resonance shielding tensors. *J. Chem. Phys.* **1996**, *104*, 5497–5509. [CrossRef]
39. Lu, T.; Chen, F. Multiwfn: A multifunctional wavefunction analyzer. *J. Comput. Chem.* **2012**, *33*, 580–592. [CrossRef]
40. Turner, M.J.; McKinnon, J.J.; Wolff, S.K.; Grimwood, D.J.; Spackman, P.R.; Jayatilaka, D.; Spackman, M.A. *Crystal Explorer 17*; University of Western Australia, 2017. Available online: <http://hirshfeldsurface.net> (accessed on 12 June 2017).
41. Foresman, J.B.; Frisch, A. *Exploring Chemistry with Electronic Structure Methods*, 2nd ed.; Gaussian: Pittsburgh, PA, USA, 1996.
42. Chang, R. *Chemistry*, 7th ed.; McGraw-Hill: New York, NY, USA, 2001.
43. Kosar, B.; Albayrak, C. Spectroscopic investigations and quantum chemical computational study of (E)-4-methoxy-2-[(p-tolylimino)methyl]phenol. *Spectrochim. Acta Part A Mol. Biomol. Spectrosc.* **2011**, *78*, 160–167. [CrossRef] [PubMed]
44. Koopmans, T.A. Ordering of wave functions and eigenenergies to the individual electrons of an atom. *Physica* **1933**, *1*, 104–113. [CrossRef]
45. Parr, R.G.; Yang, W. *Density Functional Theory of Atoms and Molecules*, 1st ed.; Oxford University Press: Oxford, UK, 1989.
46. Parr, R.G.; Szentpály, L.V.; Liu, S. Electrophilicity Index. *J. Am. Chem. Soc.* **1999**, *121*, 1922–1924. [CrossRef]

47. Singh, R.; Kumar, A.; Tiwari, R.; Rawat, P.; Gupta, V. A combined experimental and quantum chemical (DFT and AIM) study on molecular structure, spectroscopic properties, NBO and multiple interaction analysis in a novel ethyl 4-[2-(carbamoyl)hydrazinylidene]-3,5-dimethyl-1H-pyrrole-2-carboxylate and its dimer. *J. Mol. Struct.* **2013**, *1035*, 427–440. [[CrossRef](#)]
48. Kwocz, A.; Kochel, A.; Chudoba, D.; Filarowski, A. Tautomeric design of ortho-hydroxyheterocyclic Schiff bases. *J. Mol. Struct.* **2015**, *1080*, 52–56. [[CrossRef](#)]
49. Krasowska, M.; Kochel, A.; Filarowski, A. The conformational analysis of 2-hydroxyaryl Schiff thiosemicarbazones. *Cryst. Eng. Comm.* **2010**, *12*, 1955–1962. [[CrossRef](#)]
50. Bader, R.F.W. *Atoms in Molecules: A Quantum Theory*, 2nd ed.; Oxford University Press: Oxford, UK, 1994.
51. Carroll, M.T.; Chang, C.; Bader, R.F. Prediction of the structures of hydrogen-bonded complexes using the laplacian of the charge density. *Mol. Phys.* **1988**, *63*, 387–405. [[CrossRef](#)]
52. Carrol, M.T.; Chang, C.; Bader, R.F.W. An analysis of the hydrogen bond in BASE-HF complexes using the theory of atoms in molecules. *Mol. Phys.* **1998**, *65*, 695–722. [[CrossRef](#)]
53. Koch, U.; Popelier, P.L.A. Characterization of C-H-O Hydrogen Bonds on the Basis of the Charge Density. *J. Phys. Chem.* **1995**, *99*, 9747–9754. [[CrossRef](#)]
54. Espinosa, E.; Molins, E.; Lecomte, C. Hydrogen bond strengths revealed by topological analyses of experimentally observed electron densities. *Chem. Phys. Lett.* **1998**, *285*, 170–173. [[CrossRef](#)]
55. Bader, R.F.W.; Essen, H. The characterization of atomic interactions. *J. Chem. Phys.* **1984**, *80*, 1943–1960. [[CrossRef](#)]
56. Popelier, P.L.A. *Atoms in Molecules: An Introduction*; Pearson Education Limited, Edinburgh Gate: Harlow, UK, 2000.
57. Parthasarathi, R.; Subramanian, V.; Sathyamurthy, N. Hydrogen Bonding in Phenol, Water, and Phenol–Water Clusters. *J. Phys. Chem. A* **2005**, *109*, 843–850. [[CrossRef](#)]
58. Rozas, I.; Alkorta, I.; Elguero, J. Behavior of Ylides Containing N, O, and C Atoms as Hydrogen Bond Acceptors. *J. Am. Chem. Soc.* **2000**, *122*, 11154–11161. [[CrossRef](#)]
59. Espinosa, E.; Alkorta, I.; Elguero, J.; Molins, E. From weak to strong interactions: A comprehensive analysis of the topological and energetic properties of the electron density distribution involving X–H···F–Y systems. *J. Chem. Phys.* **2002**, *117*, 5529–5542. [[CrossRef](#)]